Received: 26 October 2020 | Revised: 31 December 2020 | Accepted: 18 January 2021

DOI: 10.1002/qua.26615

FULL PAPER

International Journal of QUANTUM CHEMISTRY WILEY

Ab initio dynamics of gas-phase and aqueous-phase hydrolysis of adenosine triphosphate

Raghav Saxena | V B K Sai Phani Kumar Avanigadda | Raghvendra Singh | Vishal Agarwal

Department of Chemical Engineering, Indian Institute of Technology Kanpur, Kanpur, Uttar Pradesh, India

Correspondence
Raghvendra Singh and Vishal Agarwal, Department of Chemical Engineering, Indian Institute of Technology Kanpur, Kanpur 208016, Uttar Pradesh, India.
Email: raghvend@iitk.ac.in (R. S.) and
Email: vagarwal@iitk.ac.in (V. A.)

Funding information
Indian Institute of Technology Kanpur, Grant/Award Number: Initiation Grant; Ministry of Human Resource Development, Grant/Award Number: Support for Masters student

Abstract

In this study, we have modelled the non-enzymatic hydrolysis of ATP in the gas-phase and the aqueous-phase by performing ab initio molecular dynamics simulations combined with an enhanced sampling technique. In the gas-phase, we studied hydrolysis of fully protonated ATP molecule, and in the aqueous-phase, we studied hydrolysis of ATP coordinated with: a) two H^+ ions (H-ATP), b) Mg^{2+} (Mg-ATP), and c) Ca^{2+} (Ca-ATP). We show that gas-phase ATP hydrolysis follows a two-step dissociative mechanism via a highly stable metaphosphate intermediate. The Adenine group of the ATP molecule plays a crucial role of a general base; temporarily accepting protons and thus helping in the elimination-addition process. In the aqueous-phase hydrolysis of ATP, we find that the cage of solvent molecules increases the stability of the terminal phospho-anhydride bond through a well-known cage-effect. The nature of the ions has an important effect on the mechanism of the reaction. We find a two-step dissociative-type mechanism for H-ATP, a single-step dissociative-type mechanism for Mg-ATP, and an S_N-2 type concerted hydrolysis pathway for Ca-ATP.

KEYWORDS
ATP hydrolysis, Enzymatic catalysis, Metadynamics, S_N1 dissociation

1 | INTRODUCTION

Phosphoryl transfer reactions are ubiquitous in biological systems [1, 2]. For example, signal transduction and primary metabolic pathways are hinged on the selective phosphoryl-transfer chemistry. Enzymatic hydrolysis of adenosine triphosphate (ATP) forms one such important class of biological reaction which provides energy for performing myriad of crucial functions inside our body, for example, muscle contraction, chemical synthesis and so forth [3, 4]. Enzymes help in selectively catalyzing ATP hydrolysis by providing an alternate pathway of a lower free-energy barrier. Since enzymes play such an essential role in our body, it becomes imperative to study their rate-enhancing role. Such an understanding begins by first discerning the mechanistic details and barriers of an un-catalyzed reaction—which forms the basis for further dissecting enzyme-catalyzed reactions.

Over the last couple of decades, there has been intense debate about the mechanistic aspects of non-enzymatic phosphate hydrolysis [1, 2]. The discussions revolve around two extreme cases, namely the dissociative [5–8] and the associative pathways [8, 9]. In the dissociative mechanism, terminal phospho-anhydride bond breaks before the attack of the nucleophilic water molecule. It involves the formation of a triangular planar metaphosphate-type intermediate (or transition-state). Whereas, in the associative mechanism, the attack of lytic water molecule takes place before cleavage of the terminal phospho-anhydride bond, involving the formation of a penta-coordinated trigonal bi-pyramidal phosphorus intermediate (or transition-state). Another highlighted interim reaction pathway is when the two events, that is, breaking of the terminal phospho-anhydride bond

and the nucleophile attack, take place simultaneously; therefore, aptly known as the concerted mechanism [10]. A more elaborative description of the mechanistic details can be found elsewhere [2].

Beyond the classical classification into dissociative, associative, and concerted mechanism(s); ATP hydrolysis can also be classified as a solvent-assisted or substrate-assisted mechanism. In solvent-assisted catalysis, the nearby water molecules play an active role by transferring proton via shuttling along the chain of a hydrogen-bonded network, as shown previously [5, 8]. In substrate-assisted catalysis, the substrate itself plays the role of a general base and helps in the dynamic rearrangement of protons [10, 11].

Previous studies on nucleoside triphosphate hydrolysis have shown that the triphosphate group of the molecule takes part in the reaction, however, the role of the nucleobase adenine has not been explored yet. This might be because most of the previous studies were done with simple model molecules like monophosphate esters, pyrophosphates [9, 11, 12], or truncated versions of ATP (e.g., methyl triphosphate) [5, 6, 8]; likely because of the computationally intensive nature of these calculations. Adenine group of the ATP head is a nitrogenous-base that can temporarily accept protons and help in the hydrolysis process. The specificity aspect of nucleobase may become relevant in the gas-phase or enzymes' hydrophobic pockets that adopt a closed and compact conformation and where only one water molecule is allowed to react with the ATP [13, 14]. In this article, we have modeled ATP hydrolysis in the gas-phase and the aqueous-phase by performing ab initio molecular dynamics (AIMD) simulations. We treat full ATP molecule at a quantum-mechanical level in the hope of capturing the possible role of the adenosine group in the hydrolysis process.

We study gas-phase ATP hydrolysis for several reasons. First, it forms a vital comparison to understand the role of water. We show below that the cage effect due to surrounding water molecules increases the free-energy barrier for dissociating the terminal phosphate moiety. Second, some studies in the literature suggest that ATP's conformational state attached to the enzymatic protein is very different from that in the aqueous solution. For example, Kobayashi et al. [15] compared conformations of ATP in solution to that when complexed with a protein. The authors concluded that ATP in a protein assumes a conformation rarely found in the aqueous solution. The most dominant conformer found in their study had a bent structure, making gas-phase studies a more relevant comparison. Last, as mentioned earlier, some studies have shown that ATP hydrolysis occurs in the presence of one water molecule in the enzymes' hydrophobic pockets [10, 13, 14, 16], making one water gas-phase study an appropriate reference environment for such enzymatic reactions compared to aqueous-phase, where the mechanism is known to occur via solvent-assisted proton shuttling.

Most of the previous effort concentrated on understanding the reaction chemistries and free-energy barriers for Mg-ATP hydrolysis. It is not clear how these will be affected by changing the nature of the coordinating ion. For example, how would the barriers and mechanism change by having a monovalent ion or any other divalent ion instead of Mg^{2+}. In this article, we answer these questions by comparing the hydrolysis process in the aqueous phase for—(1) ATP coordinated with H^+ ions, (2) ATP coordinated with Mg^{2+} ion, and (3) ATP coordinated with Ca^{2+} ion. We know of no previous theoretical study that modeled the hydrolysis of Ca-ATP in the aqueous solution. This will offer comparison to the well-studied Mg-ATP hydrolysis by several excellent studies before [6, 8]. The results from Ca-ATP aqueous-phase simulation will be relevant for many Ca-ATPase. Although previous studies in vacuum and solvent environment have provided several insights, a systematic study comparing gas-phase and aqueous-phase hydrolysis of ATP is still missing. The primary motivation of this work is to perform a systematic analysis comparing important parameters like water, nature of the coordinating ion, and nucleobase specificity on the ATP hydrolysis reaction. In the aqueous-phase, we treat the entire system (ATP molecule, ∼500 water molecules, and ions) at a quantum-mechanical level. The definitive treatment of every water molecule in the system revealed a well-known phenomenon called cage-effect, which directly impacted the reaction chemistries.

Exploring reactive-events in ATP hydrolysis, even in the gas-phase, is a daunting computational task. One of the reasons for this is that the un-catalyzed phosphate hydrolysis has a huge free-energy barrier. And, therefore, a brute-force AIMD simulation fails to capture the reactive-event because of the time-scale problem. The problem can be addressed by several available, accelerated MD methods [17], each having its own distinct advantage. We perform our studies using the metadynamics method [18], which enhances the probability of the hydrolysis event by slowly adding repulsive potential along certain collective variables (CV) defined in such a way to encompass the possibility of associative, dissociative, and concerted reaction pathways.

The remainder of this article is organized as follows: in Section 2 we briefly describe the methods used to generate initial ATP conformer in the gas-phase and aqueous-phase; we also offer computational details on ab-initio MD simulations and metadynamics. In Section 3, we give results and discussion on ATP hydrolysis in the gas-phase and the aqueous-phase elucidating the role of water and ions. Finally, in Section 4, we offer concluding remarks.

2 | METHODOLOGY

2.1 | System setup

ATP consists of three main components: the adenine ring, the ribose ring, and the triphosphate as shown in Figure 1. We denote the terminal phosphorous on the triphosphate as "P_γ" and the hydroxyl oxygen on this phosphorous as "$O_{\gamma s}$." We refer the reader to Figure 1 for the rest of

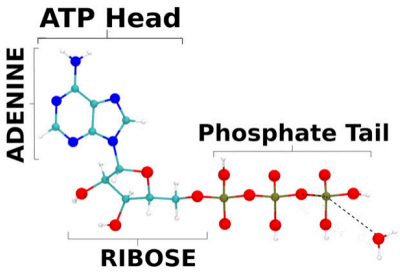

FIGURE 1 Representative figure of adenosine triphosphate (H-ATP) molecule along with a water molecule. The water oxygen is denoted as O_w. R_1 is the distance between P_γ and $O_{\beta b}$; and R_2 is the distance between O_w and P_γ. Hydrogen atoms are shown in white, oxygen atoms in red, phosphorus atoms in tan, carbon atoms in cyan and nitrogen atoms in blue

the symbols. In what follows, we denote "H-ATP" to be the state of ATP when $O_{\alpha s}$, $O_{\beta s}$ and two $O_{\gamma s}$ are coordinated with H^+ ions; "Mg-ATP" when $O_{\gamma s}$ and $O_{\beta s}$ are coordinated with Mg^{2+} ion; and "Ca-ATP" when $O_{\gamma s}$ and $O_{\beta s}$ are coordinated with Ca^{2+} ion. In our aqueous-phase simulations, *two* protons on the tri-phosphate tail leave the ATP molecule during equilibration runs and are solvated in the aqueous-phase, thus forming a divalent ion. This is in concordance with the experimental studies that ATP exists as a divalent ion at low pH values [19, 20]. At higher pH value, ATP may exist as a trivalent or a tetravalent ion which may change the reaction mechanism and barriers [21, 22]. We do not study the effect of pH in this work.

2.1.1 | Gas-phase

In the gas-phase, we only studied the hydrolysis of H-ATP. H-ATP can exists in large number of conformers in the gas-phase. We found over 800 conformers in the gas-phase by performing simulated-annealing molecular dynamics simulations using AMBER (GAFF) force-field [23] using Gabedit software package [24]. The structures (and the energies) were further refined by performing geometry optimization with PM6-DH2 method [25] in MOPAC7 software package [26]. The computational expense limits the feasibility of studying hydrolysis mechanism for each of these conformers. Moreover, the conformers span over ∼300 kJ/mol and the probability of existence of high-energy conformers is almost zilch. Therefore, we extracted conformers whose relative energies lied within 30 kJ/mol compared to the lowest energy conformer (about *seven* conformers satisfied this criteria). These conformers were further optimized with Density functional theory calculations using B3LYP/6-31+g(d) [27–31] as the model chemistry. We show comparison of electronic energies of these *seven* conformers relative to the lowest energy conformer in Figure S1. The lowest energy conformer (i.e., conformer 3 in Figure S1) was used for studying the gas-phase hydrolysis mechanism. The conformer has a bent structure which is stabilized by the intra-molecular hydrogen bonding between the adenosine-head and the phosphate-tail. For comparison, we also studied hydrolysis mechanism of a conformer which has a more open structure. Another reason for studying this conformer was that the previous experimental studies indicate presence of an open conformer in the aqueous-phase [32]. We show snapshots of these two conformers in Figure S2 and compare several dihedral angles of these conformers in Table S1.

Further, to generate an initial guess for H-ATP/water complex in the gas-phase, we performed geometry optimizations on several positions of water near the triphosphate tail. We found *six* reactant complexes as shown in Figure S3. The most stable complex was used for AIMD and metadynamics simulations.

2.1.2 | Aqueous-phase

The initial structure for ATP (coordinated with either H^+, Mg^{2+} or Ca^{2+}) in the aqueous-phase was generated by performing classical molecular dynamic simulations using GROMACS simulation package (version 2018) [33, 34]. We used SPC/E force-field [35] for the water potential and AMBER (GAFF) force-field [23] for the rest of the interactions. The force-field parameter file for GROMACS was generated using the Acpype software [36]. Following steps were used for these simulations. (a) ATP was solvated in a cubic box of 25 Å using subroutines in GROMACS, which added about 490 water molecules to the simulation box. (b) NVT molecular dynamics simulations were performed for 100 ps by keeping ATP fixed. This was done to remove any bad contacts which might have been obtained due to random insertion of water molecules. (c) The whole system (without any positional restraints on ATP) was then subjected to NPT molecular dynamics simulations for 5 ns. (d) The average box-size for the last 2 ns was used for further runs. The system was thermally equilibrated for another 100 ps by performing NVT molecular dynamics simulations. The coordinates and velocities from this run were used as an initial guess for studying ATP hydrolysis in the aqueous-phase.

The initial velocities for classical molecular dynamic simulations were obtained from Maxwell–Boltzman distribution. A time-step of 1 fs was used. System temperature was maintained at 310 K by using the Nosé–Hoover Chain thermostat [37].

2.2 | Simulation details

We used CP2K (version 5.1) software package [38] for performing all our production ab initio calculations. For benchmarking purposes, we also used Gaussian16 software package [39]. Density functional theory calculations were performed as formulated by Kohn–Sham [40–43] with PBE as the exchange-correlation functional [44]. We used an atom-centered Gaussian-type basis for wave-functions and plane wave basis for density (GPW) [45] via an efficient implementation in CP2K, namely Quickstep [46]. The core electrons were described by norm-conserving Goedecker, Teter, and Hutter (GTH) pseudo-potential [47, 48]. The wave-functions for outer electrons were expanded by triple-zeta valence basis with two set of polarization function (TZV2P) [49] for all the atoms except for Ca which was treated with double-zeta basis with one set of polarization function (DZVP) [49]. An energy cutoff of 300 Ry for the gas-phase and 380 Ry for the aqueous-phase simulations were used for an auxiliary plane wave basis set. The cutoffs were enough to converge the total energy to within 0.01 eV. *Six* electrons ($[2s^2 2p^4]$) for O atoms, *five* electrons ($[2s^2 2p^3]$) for N atoms, *five* electrons ($[3s^2 3p^3]$) for P atoms, *ten* electrons ($[2s^2 2p^6 3s^2]$) for Mg atoms, *four* electrons ($[2s^2 2p^2]$) for C atoms, and *ten* electrons ($[3s^2 3p^6 4s^2]$) for Ca atoms were treated explicitly. Dispersion corrections were taken into account by the Grimme's D3 method [50]. Mulliken scheme was used to compute charges on atoms (or group of atoms).

We performed NVT AIMD simulations based on Born-Oppenheimer approach. A time-step of 0.5 fs was used to numerically integrate the molecular dynamics equations. A cubic box of 30 Å size was used for the gas-phase simulations and a box of 25 Å size was used for the aqueous-phase simulations. Periodic boundary conditions were applied in all the three directions. Nosé–Hoover Chain thermostat [37] was used to maintain the system temperature at 310 K, which is the average temperature of the human body.

The initial coordinates for the system to study ATP hydrolysis in gas-phase and aqueous-phase were obtained by a systematic procedure as outlined above (vide supra).

2.2.1 | Metadynamics

The barriers associated with ATP hydrolysis in aqueous-phase are typically around 130 kJ/mol, which are much larger than $k_B T$ at 310 K. The reactive events are, therefore, thermally activated uncorrelated events with time-scales much greater than vibrational times; and hence termed as rare-events. To put this into perspective, we consider a hydrolysis barrier of E_{act} = 130 kJ/mol. For a pre-exponential factor of 10^{13} s^{-1}, the average time spend by the ATP in the reactant basin is $\sim 10^9$ s—which is much larger than the time-scales accessible by a brute-force AIMD simulations.

We have, therefore, used metadynamics method [18, 51–53] which slowly coaxes the system to a reactive event by adding repulsive potentials along the path of certain CV at regular intervals. The CV are chosen in such a way to describe the process of interest. We detail below the choice of CV (vide infra).

We have used the extended Lagrangian implementation of metadynamics [51] in CP2K to probe the reactive-events. In this scheme, the repulsive potentials are added along the auxiliary variables (one for each CV) of mass, m_α, which are coupled to real CV through harmonic springs of force constant, k_α.

Several functional forms for repulsive potentials has been suggested in literature. In this work, we have used the *n*-dimensional Gaussian function, where *n* is the number of CV. Since we have two CV, a two-dimensional Gaussian function acts as the repulsive potential. The free-energy was reconstructed from the history-dependent potential using the equation:

$$\Delta F(s_1,s_2) = -\lim_{t\to\infty}\int_0^t \sum_{i=1}^{d(t')} \left[w(t')\,\delta(t'-t_i)\exp\left(-\left(\frac{\left(s_1\left(\vec{R}\right)-s_1\left(\vec{R}(t')\right)\right)^2}{2\sigma_1^2} + \frac{\left(s_2\left(\vec{R}\right)-s_2\left(\vec{R}(t')\right)\right)^2}{2\sigma_2^2} \right)\right)\right] dt' \quad (1)$$

where s_1 and s_2 are the two CV. t_i is the simulation time at which the i^{th} Gaussian is added to the accumulating bias potential, $w(t')$ is the height and σ is the width of each Gaussian.

A constant Gaussian height of w = 1 kcal/mol ($\sim$1.5 $k_B T$) was used—which serves as the natural error in our simulations. A Gaussian width of σ = 0.05 for each CV was used in this work. m_α was set to 50 amu and k_α was set to 2 au to adiabatically separate the dynamics of real space variables from auxiliary variables. A Gaussian hill deposition rate of 0.05 fs^{-1} was chosen to avoid the problem of hill-surfing [54]. The parameters are chosen after several benchmarking studies as detailed in our previous work [55]; and they are similar to the ones used in the previous work on nucleoside triphosphate hydrolysis [8, 56–58]. In our previous work on cellulose (a biological molecule) pyrolysis [55], we showed that by using the recipe suggested by Ensing et al. 2005, we were able to converge the free-energy barriers of

gas-phase methyl-glucoside and cellobiose decomposition to within the Gaussian height. To go beyond that one would need to perform well-tempered metadynamics [59] which is currently too computationally expensive for the size of the system used in this work. The natural error of our metadynamics simulations, that is, the Gaussian height, will not affect the qualitative comparisons we have presented in this work.

2.2.2 | Collective variables

In this study we have used coordination number type CV. We used P–O coordination number as the CV in the metadynamics simulation which is described by the following functional form:

$$\mathrm{CN[P-O]} = \sum_{j \in O} \frac{1-\left(R_{\mathrm{PO}_j}/R^{o}_{\mathrm{PO}}\right)^{6}}{1-\left(R_{\mathrm{PO}_j}/R^{o}_{\mathrm{PO}}\right)^{12}} \tag{2}$$

where R^{o}_{PO} is distance cut off parameter which characterizes the bond between P–O. We chose a value of $R^{o}_{\mathrm{PO}} = 4.5$ a.u (~ 2.38). The following two CV were employed in this study: (a) CV1: coordination number of terminal phosphorus P_γ with bridging oxygen $O_{\beta b}$ (see Figure 1 for symbols), and (b) CV2: coordination number of terminal phosphorus P_γ with two γ oxygens, that is, $O_{\gamma s}$ and water oxygens O_{w}. For aqueous-phase study all the water oxygens were included in CV2. This choice ensures we are not biasing our reaction to one particular water molecule. The two CV were chosen to capture all the possible mechanisms of ATP hydrolysis; namely dissociative, associative and concerted. The CV used are similar to the ones used in previous studies [8, 56–58]. CV1 represents the breaking and reformation of bond between P_γ and $O_{\beta b}$, and CV2 represents the attack of nucleophilic water molecule on terminal phosphorus. We included γ oxygens into CV2 after several trial metadynamics runs. Our trial runs without γ oxygens in CV2 had proton transfer from water to γ oxygen. In the process, $O_{\gamma s}$ is released as water and O_{w} takes place of $O_{\gamma s}$ in the ATP molecule; making CV2 redundant for the reaction we want to study.

3 | RESULTS AND DISCUSSION

3.1 | Hydrolysis of H-ATP in the gas-phase

We begin by detailing the hydrolysis reaction of H-ATP in the gas-phase, where we studied the hydrolysis of H-ATP by a single water molecule. "H-ATP" refers to the state of ATP where phosphate oxygens are coordinated with H^+ ions. We refer the reader to Section 2.1 for notational details. As mentioned earlier, gas-phase studies become important in the enzymatic pocket where the environment for ATP hydrolysis is hydrophobic. Second, it becomes an important comparison to understand the role of water on the ATP hydrolysis reaction.

The restricted free energy surface computed using Equation 1 is shown in Figure 2A. From this free-energy surface, we obtain an overall free-energy barrier of 32.3 kcal/mol. The free-energy barrier for the first and the second step are 20.6 and 31.3 kcal/mol, respectively. The metadynamics simulations on the random configuration yielded similar overall barriers and reaction mechanism (see Figure S4); therefore, we do not analyze it further in this manuscript.

We note here that PBE functional is known to give an error within 0.2 eV. Also, free energy barriers might be affected by the selection of CV; therefore, we put little emphasis on the magnitude of the barriers and focus on the qualitative findings and comparisons. Additionally, we know of no gas-phase experiments of ATP hydrolysis in the literature. The predictions from our gas-phase study will be useful if such experiments are performed in the near future.

The restricted free-energy surface (see Figure 2A) shows several distinct features. The reactant (denoted as "Reac"), the intermediate (denoted as "Int"), and the product state (denoted as "Prod") can be identified from the free-energy minima. The two saddle-points on the free-energy surface are the probable transition-states (denoted as "TS1" and "TS2"): TS1 is the transition-state between the reactant and the intermediate; and TS2 is the transition-state between the intermediate and the product. The snapshots of these states are shown in Figure 4.

We also provide a movie of the gas-phase metadynamics trajectory in Figure S5. During the whole process, we observe dynamic rearrangement of the protons involving the Adenine group, water molecule, and the tri-phosphate group of the ATP molecule as detailed below (vide infra).

In order to better understand the mechanism, we monitored the evolution of CV, bond distances and angles along the metadynamics trajectory. The changes in CV1 and CV2 with metadynamics time are plotted in Figure 3. We refer the reader to Section 2.2.2 for details on CV1 and CV2. CV1 is the coordination number of the terminal phosphorus P_γ with the bridging oxygen $O_{\beta b}$. A value of CV1 near *one*, indicates a

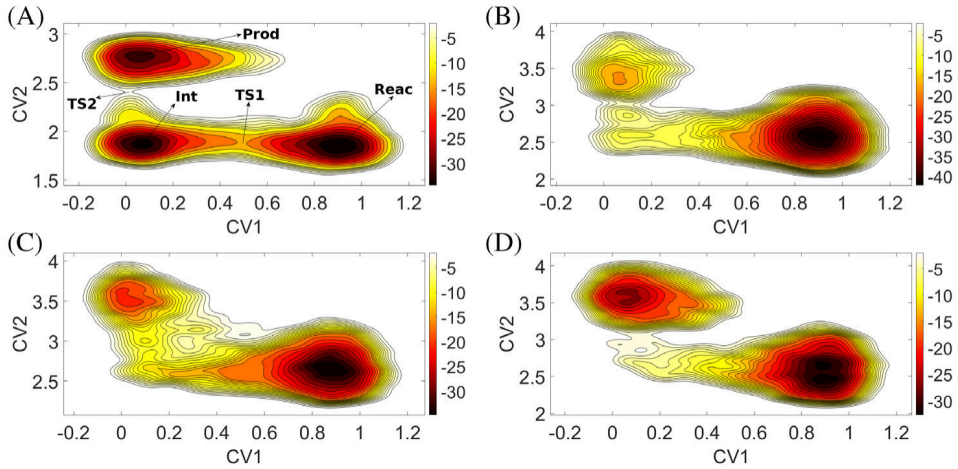

FIGURE 2 Restricted free energy surface constructed from repulsive potentials added during a metadynamics run for studying hydrolysis of (A) H-ATP in the gas-phase, (B) H-ATP in the aqueous-phase, (C) Mg-ATP in the aqueous-phase, and (D) Ca-ATP in the aqueous-phase. See Section 2.2.2 for definitions of CV1 and CV2. The figure only justifies the forward reaction barriers as the simulations were stopped before the final product basin could fully fill. The color coding for the contours are shown on the right side of the panel with units of energy in kcal/mol

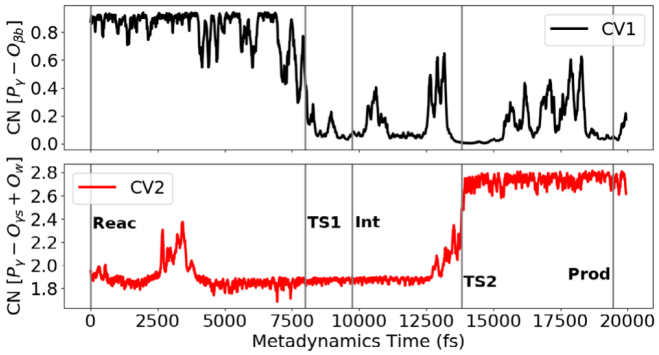

FIGURE 3 Changes in collective variables during a metadynamics run for gas-phase hydrolysis of H-ATP. See Section 2.2.2 for definitions of CV1 and CV2

chemical bond between P_γ and $O_{\beta b}$; whereas a value near *zero* represents breaking of the P_γ—$O_{\beta b}$ chemical bond. CV2 is the coordination number of terminal phosphorus P_γ with two γ oxygens and water oxygen O_w. The value of CV2 is ∼3 when water oxygen has formed a bond with P_γ; otherwise it is ∼2.

Figure 3 and the reaction trajectory (see Figure S5) shows a clear preference for the dissociative mechanism in the gas-phase. The reaction proceeds by first breaking the terminal $O_{\beta b}$—P_γ bond and then the water molecule attacking the metaphosphate. At ∼8 *ps* metadynamics time, CV1 goes from a value of ∼0.8 to ∼0.05; signifying P_γ breaking its bond with $O_{\beta b}$ and forming metaphosphate. At ∼14 *ps*, water molecule attacks the metaphosphate and water oxygen (O_w) attaches itself to P_γ to form orthophosphate. This is evident from the increase in the value of CV2 from ∼1.8 to ∼2.8, as shown in Figure 3. The reaction also involves dynamic rearrangement of protons, which is not captured with the chosen CV. However, the rearrangement of protons is clearly visible in the movie of the reactive event (see snapshots in Figure 4) and we detail this below by plotting a sum of certain coordination numbers during the metadynamics run.

It is customary to gauge the nature of the reaction mechanism (whether associative, dissociative or concerted) in ATP hydrolysis using the More O'Ferrall–Jencks (MOFJ) plot [60, 61]. The two-dimensional plot shows correlation of $O_{\beta b}$—P_γ distance with the P_γ—O_w distance. Since these distances directly relates to CV1 and CV2, the restricted free-energy surface gives us direct correlation with the MOFJ plot. For completeness, we present MOFJ plot for the gas-phase hydrolysis of H-ATP in Figure S6A. The trajectory from the upper-left corner (reactant) to the lower-right corner (product) via the upper-right corner represents the dissociative pathway; whereas, the trajectory via the lower-left corner represents the associative pathway. The trajectory via the diagonal is the concerted pathway. From the MOFJ plot in Figure S6A, it is clear that the gas-phase hydrolysis of H-ATP proceeds through the dissociative mechanism supporting our previous discussions.

At ∼8 *ps*, the first reactive event happens when P_γ parts away from the bridging oxygen, $O_{\beta b}$. This is evident from the increase in the distance between P_γ and $O_{\beta b}$ from ∼1.6 Å to more than 3 Å (see lower panel of Figure 5). Terminal phosphorus P_γ goes from tetrahedral geometry in reactant state to a planar geometry after terminal P_γ—$O_{\beta b}$ bond breaks in the intermediate state to again tetrahedral geometry after the attack of nucleophilic water molecule in the product state. We show these transitions by plotting the sum of ∠ O—P—O ($\angle\theta$) of the terminal PO_3 entity

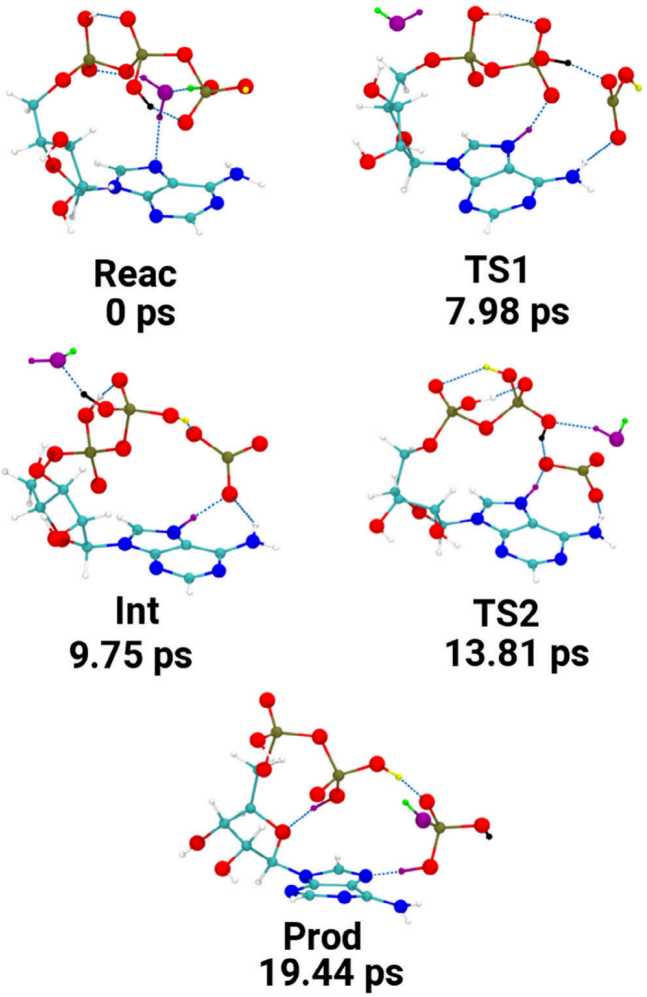

FIGURE 4 Snapshots of H-ATP hydrolysis in the gas-phase. See Figure 2A for approximate location of these snapshots in the free energy surface. Hydrogens are shown in white, oxygens in red, nitrogens in blue, carbons in cyan and phosphorous in tan. For clarity, the starting configuration of water molecule is shown in purple and the participating hydrogens in the reaction with different colors (green, black and yellow). Hydrogen bonds are also shown using dashed blue lines

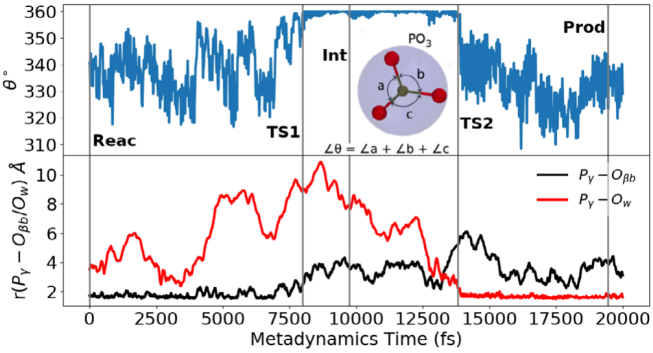

FIGURE 5 Upper panel: Changes in $\angle\theta$ during a metadynamics run for gas-phase hydrolysis of H-ATP. Lower panel: Changes in distances during a metadynamics run between P_γ and selected oxygen atoms for gas-phase hydrolysis of H-ATP. Phosphorus is shown in tan and oxygens in red. The symbols "Reac," "Int," "Prod," "TS1" and "TS2" are defined in Figure 2A

during the metadynamics run in Figure 5. After the first reactive event, the PO_3 moiety of the terminal phosphate changes its $\angle\theta$ from ~340° to ~360° indicating a change in geometry from tetrahedral to planar, and the formation of metaphosphate. From ~8 *ps* to ~14 *ps*, metaphosphate is either present as metaphosphate ion or metaphosphoric acid due to dynamic arrangement of protons. At ~14 *ps*, metaphosphate (planar geometry) converts to orthophosphate (tetrahedral geometry) after water oxygen attaches itself to the phosphorous. This is evident from the decrease in $\angle\theta$ from ~360° to 340° as shown in Figure 5.

Interestingly, metadynamics trajectory predicts presence of an intermediate with a highly stabilized metaphosphate ion (only ~1 kcal/mol higher in free-energy than the reactant configuration). Since, free-energy includes contributions from entropy; therefore, we also extracted coordinates of Reac (at 0 ps), Int (at ~9.75 ps) and Prod (at ~19.44 ps) and subjected them to geometry optimization. We plot electronic energies of Reac, Int, and Prod along with their optimized structures in Figure 6. Indeed, we do find a stable intermediate with metaphosphate ion in the gas-phase, however, it is ~21.2 kcal/mol higher in energy than the reactant state—which is much higher than the free-energy difference. This can be explained on the basis that when metaphosphate breaks from the ATP molecule, *six* vibrational degrees of freedom are converted to *three*

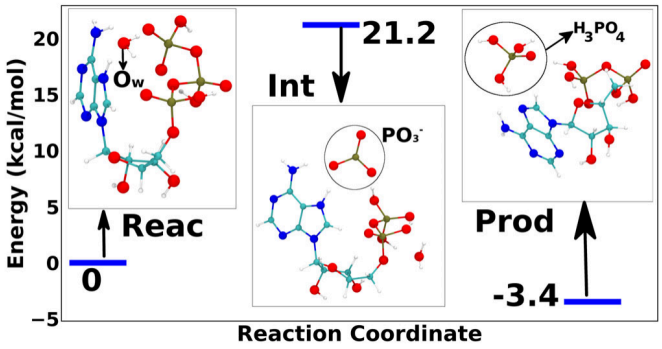

FIGURE 6 Energy profile for gas-phase ATP hydrolysis. The reactant complex is taken as the zero of energy. Also shown are optimized geometries of gas-phase reactant (Reac), intermediate (Int) and product (Prod) states. Hydrogens are shown in white, oxygens in red, nitrogens in blue, carbons in cyan and phosphorous in tan. The symbols "Reac," "Int," and "Prod" are defined in Figure 2A

translational and *three* rotational degrees of freedom; hence, increasing its entropy. The gain in entropy stabilizes the metaphosphate intermediate in the gas-phase. We mention in passing that several previous theoretical studies have shown that gas-phase hydrolysis of phosphates proceeds through a dissociative mechanism involving a formation of metaphosphate ion as a stable intermediate [9, 62, 63].

We also find that the adenosine group plays a crucial role in the hydrolysis of ATP in the gas-phase, by providing a pseudo-solvation environment. Thus, stabilizing the reaction intermediate and facilitating hydrolysis of ATP by promoting intra-molecular hydrogen transfer. This is evident from the long-range proton-shuttling involving a nitrogen atom (in the five-membered ring) from the Adenine group, the nucleophilic water molecule and the γ- and β-oxygens of the tri-phosphate group observed during the metadynamics run. Nitrogen in the five-membered ring of the Adenine group acts as the temporary resting place for the proton from the water molecule or the tri-phosphate group; thus helping in the dynamic rearrangement and transfer of proton. In order to capture the long-range motion of the protons, we plot the sum of coordination number of oxygen atoms involved in this process (denoted as O1, O2, O3 and O4 in Figure 7) with the hydrogens (denoted as H1, H2, H3 and H4 in Figure 7) that are involved in the process. We define the O—H coordination in the caption of Figure 7. Initially at T1 = 0 fs, the hydrogens are placed on the native oxygens, that is; H1 is bonded with O1; H2 and H3 are bonded with O2 (or water oxygen, O_w); and H4 is bonded with O4. Hence, the coordination-number has its maximum value of ∼3. At T2 ∼ 3000 fs, there is a drop in the O—H coordination number from ∼1 to ∼0. This happens because there is transfer of H3 from O2 to the nitrogen atom of the Adenine ring, H4 from O4 to O2, and H1 from O1 to O3. Similarly, we show several intermediate structures during the gas-phase ATP hydrolysis in Figure 7 depicting various proton transfer events.

3.2 | Hydrolysis of H-ATP in the aqueous-phase

We now elaborate on the findings of H-ATP hydrolysis in the aqueous phase. Although, we began this study with a fully protonated ATP molecule, after ab initio MD equilibration only two protons on the γ oxygens were left and rest of them were solvated in the aqueous solution (see snapshot "1" in Figure 8). This suggests that H-ATP in these conditions tends to exist as divalent ions in the bulk solution. At higher pH conditions it may be present as a trivalent or a tetravalent ion [19, 20, 64].

We plot the restricted free-energy surface for the aqueous-phase hydrolysis of H-ATP in Figure 2B obtained by performing metadynamics simulation along certain CV. We define the *two* CV used in this study in Section 2.2.2. CV1 is related to the breaking and re-formation of bond between P_γ—$O_{\beta b}$ and CV2 is related to the attack of nucleophilic water molecule. In the aqueous-phase simulations it could be any one of the water molecules surrounding the H-ATP molecule.

Unlike the gas-phase simulations, the free-energy surface obtained in the aqueous phase simulations is extremely rugged; which can be attributed to the presence of solvent coordinates in CV2. We find an overall barrier of ∼37.7 kcal/mol for the aqueous-phase hydrolysis of H-ATP—which is ∼5 kcal/mol higher than the gas-phase simulations. This can be explained on the basis of well-known "cage-effect" [65, 66], which we elaborate below. The cage-effect also leads to a much higher free-energy barrier for the first-step in the aqueous-phase hydrolysis (∼33.5 kcal/mol) compared to the gas-phase hydrolysis (∼20.6 kcal/mol).

We find that the free-energy barrier for the second step of the aqueous-phase hydrolysis (∼5.3 kcal/mol) is much smaller than the gas-phase hydrolysis (∼31.3 kcal/mol). This is because, the attacking water molecule in the gas-phase hydrolysis has an extremely large entropic space to maneuver before it attaches itself to the metaphosphate. On the other hand, the leaving metaphosphate in the aqueous-phase hydrolysis is surrounded by the "cage" of reactant water molecules which increases the probability of reacting and forming the orthophosphate product.

To better understand the mechanism of aqueous-phase H-ATP hydrolysis, we plot various parameters (such as CV, angles etc.) during the metadynamics trajectory. We also provide movie of the metadynamics trajectory in Figure S7. Just like the gas-phase simulations, we observe dynamic rearrangement of the protons. However, in the aqueous-phase simulations it is the surrounding water molecules which play an active role instead of the adenosine group. The proton diffuses in the solvent through Grotthuss mechanism [67]. At different instances of time, we

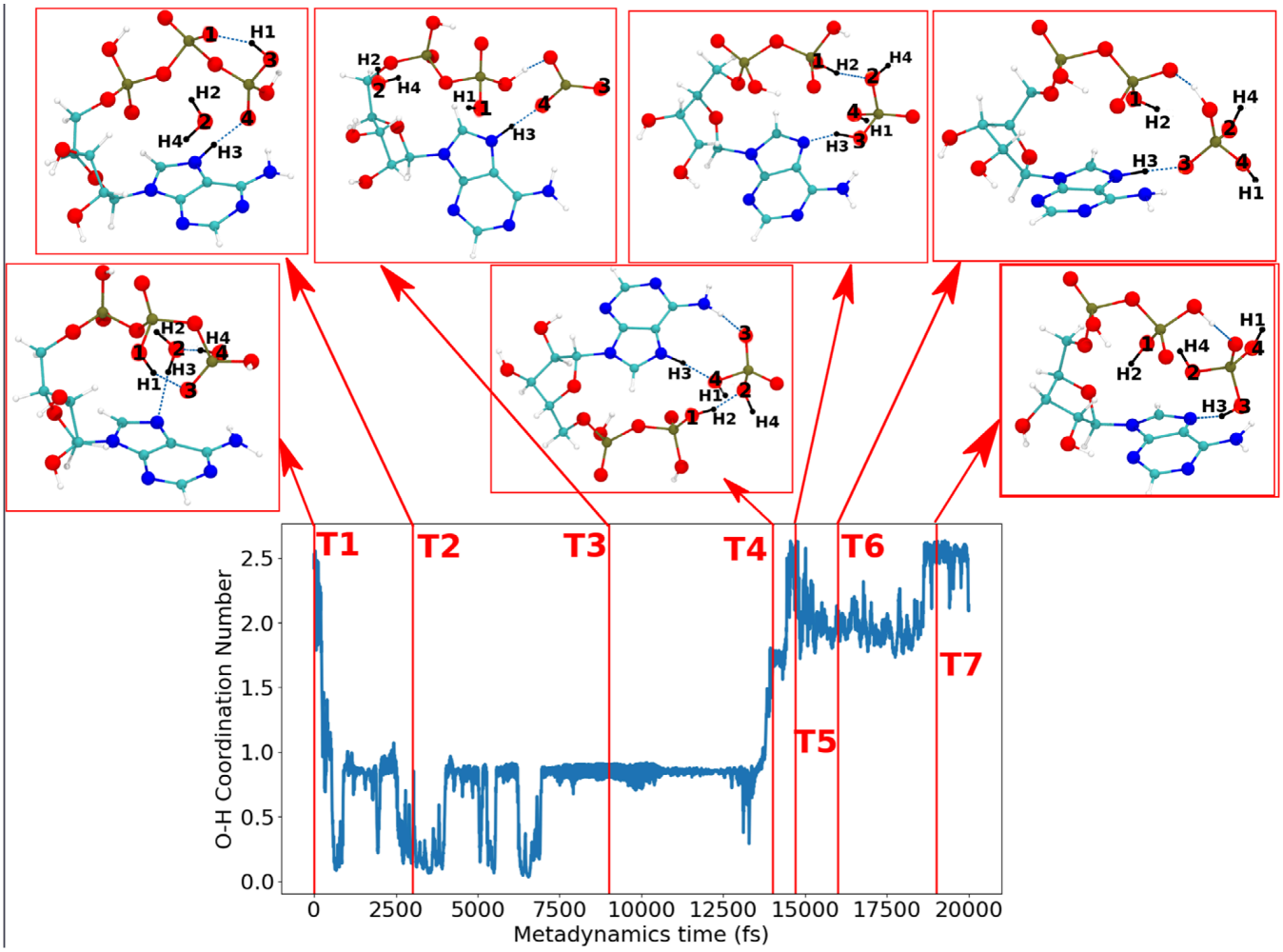

FIGURE 7 Plot of O—H coordination number versus metadynamics time. We also show snapshots of the complex at various times during the simulation. The O—H coordination is the sum of the coordination numbers: CN(O1;{H1, H2}) + CN(O4;{H4, H1}) + CN(O2;H3) + CN(O3;H3). $CN[O-H] = \sum_{j \in H} \frac{1-\left(R_{OH_j}/R^o_{OH}\right)^6}{1-\left(R_{OH_j}/R^o_{OH}\right)^{12}}$. The relevant oxygens and hydrogens are numbered in the snapshots

observe the formation of Zundel cation [68] and Eigen cation [69]. The complex nature of the hydrated proton has been well documented before [70].

We plot the evolution of CV versus metadynamics simulation time in Figure 9. And, we also plot the sum of ∠ O—P—O ($\angle\theta$) of the terminal PO_3 entity versus metadynamics time in Figure 10. Unlike the gas-phase simulations, both Figures 9 and 10 show large fluctuations in CV1 and $\angle\theta$, respectively. CV1 fluctuates between a value of ∼0.9 to ∼0.2 several times in between 9 to 18.5 ps of the metadynamics time. At the same instances, the $\angle\theta$ fluctuates between ∼340° to 360°. This suggests that P_γ—$O_{\beta b}$ bond breaks and reforms—and terminal PO_3 goes from a tetrahedral geometry to a planar geometry—several times during this period. We show these events in Figure 8 (snapshots "2" and "3"). In the gas-phase study, once P_γ—$O_{\beta b}$ bond breaks, we observe no recombination between the two dissociated species. This is because once the molecule has gained enough energy to leave, there is no motivation for it to go back. However, in the aqueous-phase hydrolysis, the dissociated species collides with the solvent molecules; and therefore have the tendency to come back and recombine. This process of leaving and recombining occurs until the intermediate makes its way through the solvent. The phenomena is known as "cage-effect" [71]. Thus, the high free energy barrier for the first step in the case of aqueous-phase hydrolysis compared to the hydrolysis in the gas-phase can be attributed to the cage-effect.

At ∼18.79 ps, P_γ finally breaks its bond with $O_{\beta b}$ as indicated by the decrease in CV1 from ∼0.8 to ∼0.1 (see Figure 9 and snapshot "4" in Figure 8). At the same instant, as shown in Figure 10, $\angle\theta$ goes from ∼340° to 360°, that is, a planar metaphosphate is formed. The lytic water loses its proton to the bridging oxygen, $O_{\beta b}$, and is involved in a network of hydrogen bond with two assisting water molecules (shown in yellow and green in snapshot "5" of Figure 8) and one of the γ oxygens.

At ∼21.74 ps, the lytic water finally attaches itself to metaphosphate to form orthophosphate, losing its proton to the nearby water molecule (shown in yellow in snapshot "6" of Figure 8). At ∼22.35 ps, the orthophosphate ion gains protons from the solvent molecules to finally form

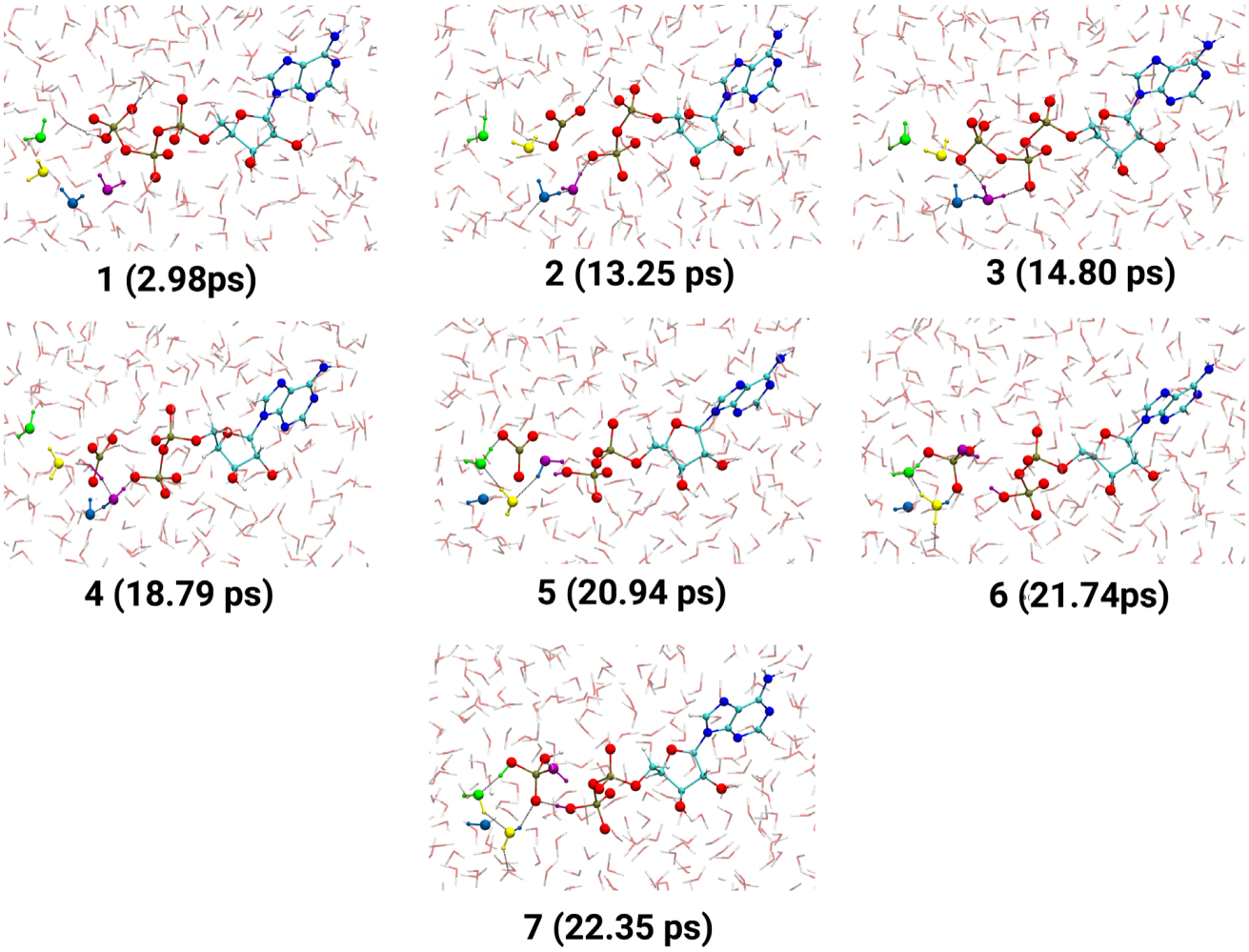

FIGURE 8 Snapshots of H-ATP hydrolysis in aqueous solution during a metadynamics run. We use the following color coding to depict atoms: Hydrogens in white, oxygens in red, nitrogens in blue, carbons in cyan, and phosphorus in tan. Lytic water molecule finally attacking the metaphosphate is shown in purple and the assisting water molecules are shown in blue, yellow and green. For clarity, all the other water molecules are blurred. Some hydrogen bonds are also shown using dashed black lines

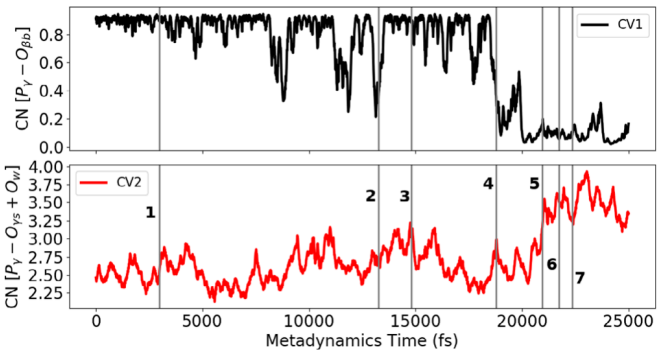

FIGURE 9 Evolution of collective variables during hydrolysis of H-ATP in the aqueous solution. See Section 2.2.2 for definitions of CV1 and CV2. The snapshots for the numbered times are shown in Figure 8

orthophosphoric acid (see snapshot "7" in Figure 8). The mechanism explained above is consistent with the solvent-assisted catalysis where nearby water molecules plays a role of general base helping in dynamic rearrangement of protons; in agreement with the previous studies [5, 8].

Figures 9 and 10 suggest that the metaphosphate intermediate is present for an extremely short period of time. Therefore, it is difficult to discern between dissociative and concerted mechanism. However, Figures 9 and 10 also suggest that a metaphosphate intermediate is formed first and then the lytic water attaches itself to metaphosphate, pointing towards S_N1-type dissociative mechanism in the aqueous-phase. This is also

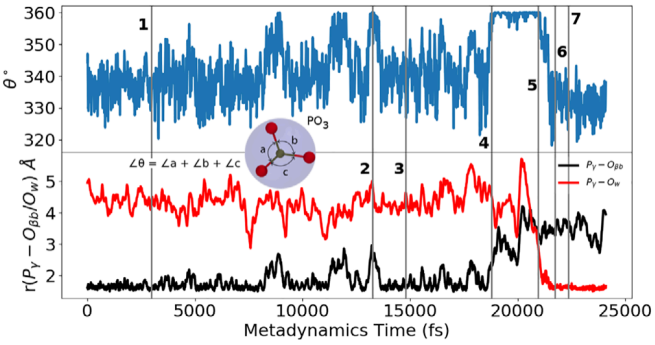

FIGURE 10 Upper panel: Changes in $\angle\theta$ during a metadynamics run for aqueous-phase hydrolysis of H-ATP. Lower panel: Changes in distances during a metadynamics run between P_γ and selected oxygen atoms for aqueous-phase hydrolysis of H-ATP. Phosphorus is shown in tan and oxygens in red. The snapshots for the numbered times are shown in Figure 8

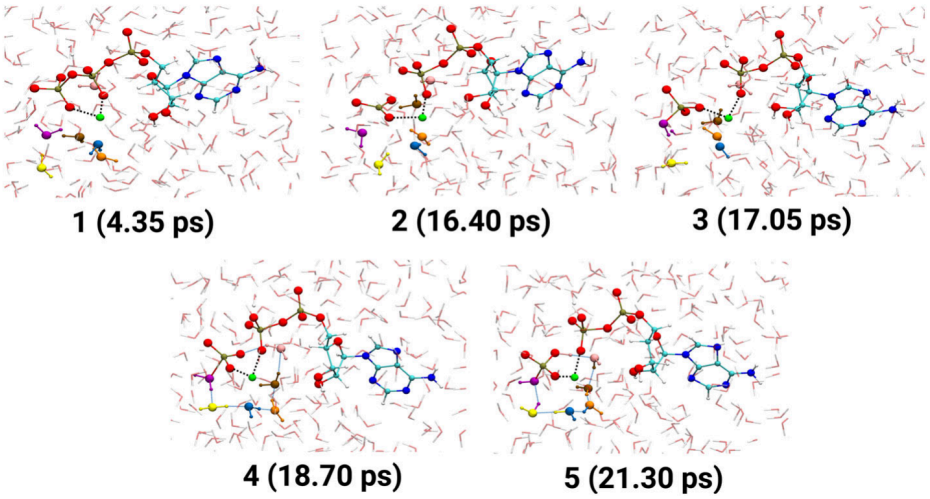

FIGURE 11 Snapshots of Mg-ATP hydrolysis in aqueous solution during a metadynamics run. We use the following color coding to depict atoms: Magnesium in green, hydrogens in white, oxygens in red, nitrogens in blue, carbons in cyan, and phosphorus in tan. Lytic water molecule finally attacking the metaphosphate is shown in purple and the assisting water molecules are shown in yellow, blue, orange, brown, and pink. For clarity, all the other water molecules are blurred. Some hydrogen bonds are also shown using dashed blue lines

supported by the MOFJ plot shown in Figure S6B. Several experimental studies have also suggested a dissociative, metaphosphate-like transition state for phosphate hydrolysis in the aqueous solution [72, 73].

3.3 | Hydrolysis of Mg-ATP and Ca-ATP in the aqueous-phase

We now present our findings of Mg-ATP and Ca-ATP hydrolysis in the aqueous-phase. Both Mg and Ca ions are found to coordinate with ATP in our body [74]. In these simulations we replace two H^+ ions—one on the γ oxygen and the other on β oxygen of the triphosphate tail—with the divalent ions. As before, we find that the triphosphate tail loses its protons to the bulk solvent during the equilibration runs to form a divalent ion. Interestingly, after the equilibration runs, Mg ion remains chelated to the γ and β oxygens (see snapshot "1" in Figure 11); whereas Ca ion shifts to β and α oxygens (see snapshot "1" in Figure 12). A possible reason for this is that Mg and Ca ions prefer to have different coordination with the nucleophilic water oxygens in the aqueous-phase. The hydrated Mg ions is usually found to be six-coordinate with an average Mg—O distance of 2.09 Å, in an octahedron configuration, in the aqueous solution; whereas Ca ion is found to be eight-coordinate with an average Ca—O distance of 2.42 Å, in a square antiprism configuration [75–78]. Because of the larger size of Ca ion it prefers to fit into the pocket of β and α oxygens.

Similar to the previous study [8], we find that Mg(II) ion remains chelated to the γ and β oxygens throughout the hydrolysis process. Whereas, Ca(II) ion changed its chelation from bidentate to mono-dentate during the process. Also, we find both Mg and Ca ions maintained its coordination with the oxygens throughout the process. Mg ion showed an average coordination of *six*, whereas Ca ion showed an average coordination of *seven* with the nearby oxygens. This is evident from the sharp radial distribution peaks and coordination number plots in Figures S9–S11. We find an average Mg—O distance of 2.1 Å and an average Ca—O distance of 2.41 Å, agreeing well with the experimental values of average coordination distances in the aqueous-phase [75–78].

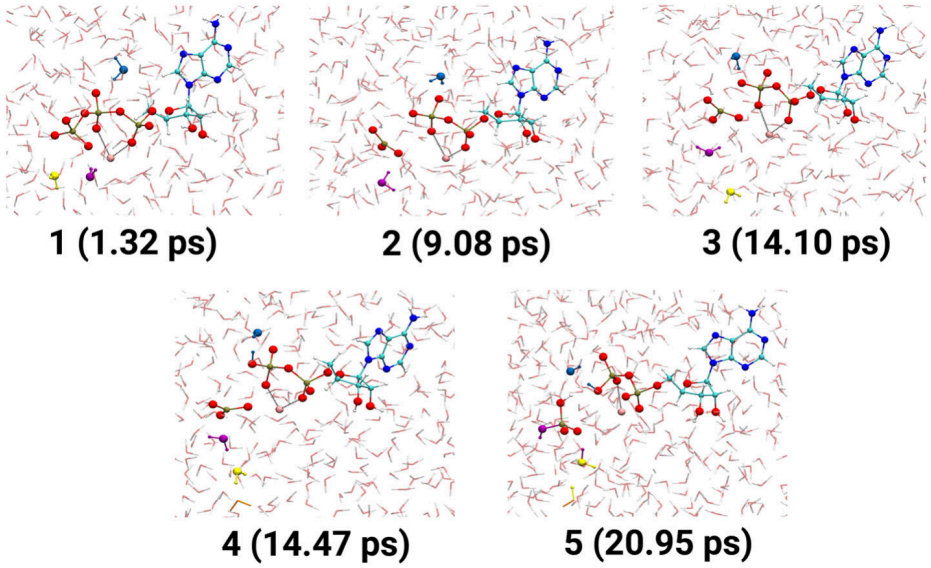

FIGURE 12 Snapshots of Ca-ATP hydrolysis in aqueous solution during a metadynamics run. We use the following color coding to depict atoms: Calcium in pink, hydrogens in white, oxygens in red, nitrogens in blue, carbons in cyan, and phosphorus in tan. Lytic water molecule finally attacking the metaphosphate is shown in purple and the assisting water molecules are shown in yellow and blue. For clarity, all the other water molecules are blurred

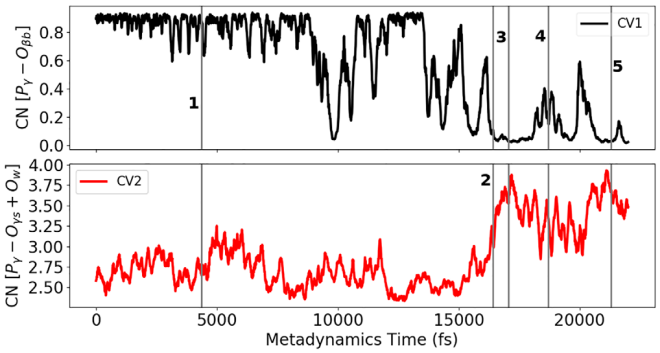

FIGURE 13 Evolution of collective variables during hydrolysis of Mg-ATP in the aqueous solution. See Section 2.2.2 for definitions of CV1 and CV2. The snapshots for the numbered times are shown in Figure 11

We present the restricted free-energy surface for the aqueous-phase hydrolysis of Mg-ATP and Ca-ATP in Figure 2C,D, respectively. The CV along which the repulsive potentials are added are defined in Section 2.2.2. We find an overall barrier of ∼30.6 and ∼30.3 kcal/mol, respectively, for the hydrolysis of Mg-ATP and Ca-ATP. Because the difference in barriers is within the natural error of 1 kcal/mol in our metadynamics simulations, we are not able to decide which one has a lower barrier. Additionally, we do not compare these barriers to experimental results because of several reasons. First, it is difficult to emulate exact experimental conditions in simulations. Second, PBE functional used in this work is accurate to within 0.2 eV. Third, the quantum effects associated with proton transfer are not accounted for in this work. Therefore, we focus on qualitative findings and comparisons rather than quantitative aspects of the simulation. We, however, mention in passing that previous experimental studies report a barrier between 26 and 31 kcal/mol [21, 79, 80] and previous in-silico studies report a barrier between 29 and 35 kcal/mol [5–10] for the non-enzymatic hydrolysis of tri-phosphates in the aqueous-phase.

Unlike the gas-phase and the aqueous-phase H-ATP simulations, we find that the reaction proceeds in a single-step and no intermediate is observed in the aqueous-phase hydrolysis of Mg-ATP and Ca-ATP. However, we find that several features of the free-energy surface are similar to the aqueous-phase H-ATP simulations. First, the free-energy surface is quite rugged in comparison to the gas-phase hydrolysis which can be attributed to the solvent coordinates. Second, the barrier for the first-step (or the only step) is much higher than the gas-phase hydrolysis process. This is due to the presence of cage of reactant water molecules which collides with the dissociated metaphosphate causing it to go back and recombine. After several attempts, the metaphosphate is finally able to gain enough energy to make its way through the cage.

We now elaborate on the mechanistic aspects of hydrolysis by plotting evolution of collective variables in Figures 13 and 14 for Mg and Ca ions, respectively. We also provide snapshots at different instances of metadynamics time in Figures 11 and 12 along with movies of the

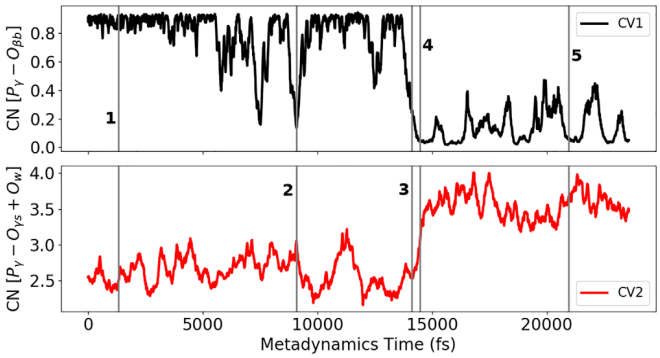

FIGURE 14 Evolution of collective variables during hydrolysis of Ca-ATP in the aqueous solution. See Section 2.2.2 for definitions of CV1 and CV2. The snapshots for the numbered times are shown in Figure 12

metadynamics trajectory in Figures S12 and S13. Similar to the aqueous-phase hydrolysis of H-ATP, we find nearby water molecules assisting in the hydrolysis process by facilitating dynamic rearrangement of protons. For example, we refer the reader to Figure 11 where we show snapshots of metadynamics trajectory for the hydrolysis of Mg-ATP. At ∼17.05 ps, the lytic water (shown in purple) attaches itself to metaphosphate ion forming an orthophosphate moiety (snapshot "3"), and gets involved in a network of hydrogen bond with five other water molecules (shown in yellow, blue, orange, brown, and pink in snapshot "4"). The proton diffuses through Grotthuss mechanism along a chain of *five* water molecules to the oxygen of the HPO_4^{2-} ion (snapshot "5").

CV1 is directly related to the terminal phospho-anhydride bond (P_γ—$O_{\beta b}$), and large fluctuations of CV1 suggests breaking and reformation of the P_γ—$O_{\beta b}$ bond, which is the characteristic of well-known "cage effect." Similar to H-ATP hydrolysis in the aqueous solution, our results show cage-effect in the hydrolysis of Mg-ATP and Ca-ATP, evident from the large fluctuations of CV1 as shown in Figures 13 and 14; respectively.

Similar to the aqueous-phase hydrolysis of H-ATP, it is difficult to discern between dissociative and concerted mechanism in case of Mg-ATP and Ca-ATP. However, as argued before, Figure 13 suggests breaking of terminal phospho-anhydride bond first and then attack of nucleophilic water, pointing toward a possible S_N1-type dissociative mechanism in the aqueous-phase hydrolysis of Mg-ATP. In contrast, in the case of aqueous-phase hydrolysis of Ca-ATP, Figure 14 shows both breaking of terminal phospho-anhydride bond and attack of lytic water happens simultaneously, indicating to a possible concerted mechanism. At ∼14.10 ps, the distance between P_γ and $O_{\beta b}$ is nearly equal to the distance between the P_γ and O_w of the lytic water. At the same instant the geometry of the leaving metaphosphate is planar (see Figure S15), which is the signature of Walden's inversion or S_N2-type concerted mechanism. These conclusions are well supported by the MOFJ plots in Figure S6C,D. For hydrolysis of Mg-ATP, the reactive trajectory is toward the dissociative corner in MOFJ plot. Whereas, the reactive event proceeds through the diagonal of the MOFJ plot in the case of hydrolysis of Ca-ATP.

The overall barriers for the aqueous-phase hydrolysis of divalent ions are much lower than the aqueous-phase (∼38 kcal/mol) hydrolysis of H-ATP suggesting a clear catalytic effect of the divalent ions. A possible reason for this is the increased electrophilicity of the terminal PO_3 after breaking of the terminal phospho-anhydride bond. This is evident from the Figures S16 and S17 which shows that the charge on the terminal PO_3 moiety becomes less negative every time P_γ—$O_{\beta b}$ bond breaks; making it easy for the nucleophilic water molecule to attack. This was not observed in the case of aqueous-phase hydrolysis of H-ATP (see Figure S8). The discussion above suggests that divalent ions facilitate the attack of the nucleophilic water molecule which is in agreement to previous computational [81, 82] and experimental studies [64, 83, 84].

4 | SUMMARY AND CONCLUSIONS

In this work, we study the hydrolysis of ATP in the gas-phase and the aqueous-phase by performing ab initio MD simulations with an enhanced sampling technique. In the gas-phase, we studied hydrolysis of fully protonated ATP molecule. In the aqueous-phase, we studied hydrolysis of ATP coordinated with: (a) *two* H^+ ions (H-ATP), (b) Mg^{2+} (Mg-ATP) and (c) Ca^{2+} (Ca-ATP).

We found that hydrolysis in the gas-phase proceeds via dissociative mechanism through a stable metaphosphate ion. Interestingly, we found that the adenosine group of the ATP molecule plays a crucial role during the hydrolysis reaction. The Adenine group played the role of a general base by accepting a proton from the water molecule, which in turn accepts the proton from the leaving metaphosphate group; thus helping in the dissociation of the ATP molecule. The final proton transfer to the phosphate oxygen occurs similarly involving the nitrogen on the Adenine ring, orthophosphate moiety and the β-phosphate oxygen. These results suggest that small molecules like monophosphate esters, pyrophosphates and truncated versions like MTP (methyl triphosphate) may not serve as good models for studying hydrolysis of ATP, GTP, and similar nucleotides; especially in an enzymatic pocket where the environment for hydrolysis is hydrophobic and is similar to the gas-phase environment.

On comparison of our gas-phase study with that of aqueous-phase hydrolysis of H-ATP, we observed several differences. First, the presence of cage of solvent molecules increases the stability of the terminal phospho-anhydride bond. The leaving metaphosphate moiety recombined with the bridging oxygen many times before finally getting captured by a nucleophilic water molecule. This was also the reason for higher free-energy

barrier for the first step for ATP hydrolysis in the aqueous solution compared to that in the gas-phase. Second, although we found that hydrolysis of both H-ATP in the gas-phase and the aqueous solution proceeded via S_N1-type dissociative mechanism involving formation of a metaphosphate intermediate; however, in the case of aqueous-phase the lifetime of the intermediate was much shorter than that in the gas-phase. Third, in the aqueous-phase, we found that the solvent plays an active role in assisting the hydrolysis process by proton transfer through Grotthuss mechanism. In contrast, in the gas-phase, we found that the Adenine group of the ATP molecule play an active role as a base helping in the hydrolysis process.

We obtained much lower free-energy barriers for the aqueous-phase hydrolysis of ATP coordinated with divalent ions (Mg^{2+} and Ca^{2+}) compared to that in the aqueous-phase hydrolysis of ATP coordinated with only H^+ ions—which suggests a clear catalytic effect of the divalent ions. This can be attributed to the increased electrophilicity of the leaving PO_3 moiety in the case of divalent ions, which facilitates attack of the nucleophilic water molecule. Interestingly, we find a single-step dissociative-type mechanism for Mg-ATP, whereas, the hydrolysis in case of Ca-ATP proceeded through an S_N-2-type concerted pathway.

ACKNOWLEDGMENTS

We acknowledge support from the High Performance Computing center at IITK. Vishal Agarwal acknowledges the funding support from Indian Institute of Technology Kanpur (initiation grant). Raghav Saxena acknowledges the financial support from the Ministry of Human Resource Development, Govt of India. We also thank Prof. Nisanth N. Nair and Prof. Sanjeev Garg for stimulating discussions on this topic.

AUTHOR CONTRIBUTIONS

Raghav Saxena: Data curation; formal analysis; investigation; visualization; writing-original draft. **Phani Kumar Avanigadda:** Data curation; writing-original draft. **Raghvendra Singh:** Conceptualization; project administration; resources; supervision. **Vishal Agarwal:** Conceptualization; methodology; project administration; resources; supervision; writing-review and editing.

DATA AVAILABILITY STATEMENT

The data that support the findings of this study are available from the corresponding author upon reasonable request.

ORCID

Raghav Saxena https://orcid.org/0000-0001-9850-0158
V B K Sai Phani Kumar Avanigadda https://orcid.org/0000-0003-0810-3103
Raghvendra Singh https://orcid.org/0000-0002-2398-8926
Vishal Agarwal https://orcid.org/0000-0001-8581-4780

REFERENCES

[1] S. C. Kamerlin, P. K. Sharma, R. B. Prasad, A. Warshel, *Q. Rev. Biophys.* **2013**, *46*, 1.
[2] J. K. Lassila, J. G. Zalatan, D. Herschlag, *Annu. Rev. Biochem.* **2011**, *80*, *669*.
[3] A. L. Buchachenko, D. A. Kuznetsov, N. N. Breslavskaya, *Chem. Rev.* **2012**, *112*, 2042.
[4] J. E. Walker, *Biochem. Soc. Trans.* **2013**, *41*, 1.
[5] B. L. Grigorenko, A. V. Rogov, A. V. Nemukhin, *J. Phys. Chem. B* **2006**, *110*, 4407.
[6] J. Akola, R. Jones, *J. Phys. Chem. B* **2003**, *107*, 11774.
[7] C. B. Harrison, K. Schulten, *J. Chem. Theory Comput.* **2012**, *8*, 2328.
[8] R. Glaves, G. Mathias, D. Marx, *J. Am. Chem. Soc.* **2012**, *134*, *6995*.
[9] Y. N. Wang, I. A. Topol, J. R. Collins, S. K. Burt, *J. Am. Chem. Soc.* **2003**, *125*, 13265.
[10] C. Wang, W. Huang, J.-L. Liao, *J. Phys. Chem. B* **2015**, *119*, 3720.
[11] F. Duarte, J. Åqvist, N. H. Williams, S. C. Kamerlin, *J. Am. Chem. Soc.* **2015**, *137*, 1081.
[12] W. Li, T. Rudack, K. Gerwert, F. Gräter, J. Schlitter, *J. Chem. Theory Comput.* **2012**, *8*, 3596.
[13] M. L. Oldham, J. Chen, *Proc. Natl. Acad. Sci. USA* **2011**, *108*, 15152.
[14] R. J. Dawson, K. P. Locher, *Nature* **2006**, *443*, 180.
[15] E. Kobayashi, K. Yura, Y. Nagai, *Biophysics* **2013**, *9*, 1.
[16] M. Prieß, H. Göddeke, G. Groenhof, L. V. Schäfer, *ACS Cent. Sci.* **2018**, *4*, 1334.
[17] M. Tuckerman, *Statistical Mechanics: Theory and Molecular Simulation*, Oxford University Press, New York **2010**.
[18] A. Laio, M. Parrinello, *Proc. Natl. Acad. Sci. USA* **2002**, *99*, 12562.
[19] R. Tribolet, H. Sigel, *Eur. J. Biochem.* **1988**, *170*, 617.
[20] P. Wang, J. L. Oscarson, R. M. Izatt, G. D. Watt, C. D. Larsen, *J. Solution Chem.* **1995**, *24*, 989.
[21] M. Taqui Khan, M. Srinivas Mohan, *J. Inorg. Nucl. Chem.* **1974**, *36*, 707.
[22] S. Meyerson, E. S. Kuhn, F. Ramirez, J. F. Marecek, *J. Am. Chem. Soc.* **1982**, *104*, 7231.
[23] J. Wang, R. M. Wolf, J. W. Caldwell, P. A. Kollman, D. A. Case, *J. Comput. Chem.* **2004**, *25*, 1157.
[24] A.-R. Allouche, *J. Comput. Chem.* **2011**, *32*, 174.
[25] M. Korth, M. Pitoňák, J. Řezáč, P. Hobza, *J. Chem. Theory Comput.* **2010**, *6*, 344.

[26] J. J. P. Stewart, *J. Comput.-Aided Mol. Des.* **1990**, *4*, 1.
[27] A. D. Becke, *Phys. Rev. A* **1988**, *38*, 3098.
[28] C. T. Lee, W. T. Yang, R. G. Par, *Phys. Rev. B* **1988**, *37*, 785.
[29] B. Miehlich, A. Savin, H. Stoll, H. Preuss, *Chem. Phys. Lett.* **1989**, *157*, 200.
[30] G. A. Petersson, M. A. Al-Laham, *J. Chem. Phys.* **1991**, *94*, 6081.
[31] G. A. Petersson, A. Bennett, T. G. Tensfeldt, M. A. Al-Laham, W. A. Shirley, J. Mantzaris, *J. Chem. Phys.* **1988**, *89*, 2193.
[32] T. Miyazaki, Y. Kameda, Y. Umebayashi, H. Doi, Y. Amo, T. Usuki, *J. Solution Chem.* **2014**, *43*, 1487.
[33] E. Lindahl, B. Hess, D. Van Der Spoel, *Mol. Model. Annu.* **2001**, *7*, 306.
[34] H. J. C. Berendsen, D. van der Spoel, R. van Drunen, *Comput. Phys. Commun.* **1995**, *91*, 43.
[35] H. Berendsen, J. Grigera, T. Straatsma, *J. Phys. Chem.* **1987**, *91*, 6269.
[36] A. W. S. da Silva, W. F. Vranken, *BMC Res. Notes* **2012**, *5*, 367.
[37] D. J. Evans, B. L. Holian, *J. Chem. Phys.* **1985**, *83*, 4069.
[38] J. Hutter, M. Iannuzzi, F. Schiffmann, J. Vandevondele, *Wiley Interdiscip. Rev. Comput. Mol. Sci.* **2014**, *4*.
[39] M. J. Frisch, G. W. Trucks, H. B. Schlegel, G. E. Scuseria, M. A. Robb, J. R. Cheeseman, G. Scalmani, V. Barone, B. Mennucci, G. A. Petersson, H. Nakatsuji, M. Caricato, X. Li, H. P. Hratchian, A. F. Izmaylov, J. Bloino, G. Zheng, J. L. Sonnenberg, M. Hada, M. Ehara, K. Toyota, R. Fukuda, J. Hasegawa, M. Ishida, T. Nakajima, Y. Honda, O. Kitao, H. Nakai, T. Vreven, J. A. Montgomery Jr., J. E. Peralta, F. Ogliaro, M. Bearpark, J. J. Heyd, E. Brothers, K. N. Kudin, V. N. Staroverov, R. Kobayashi, J. Normand, K. Raghavachari, A. Rendell, J. C. Burant, S. S. Iyengar, J. Tomasi, M. Cossi, N. Rega, J. M. Millam, M. Klene, J. E. Knox, J. B. Cross, V. Bakken, C. Adamo, J. Jaramillo, R. Gomperts, R. E. Stratmann, O. Yazyev, A. J. Austin, R. Cammi, C. Pomelli, J. W. Ochterski, R. L. Martin, K. Morokuma, V. G. Zakrzewski, G. A. Voth, P. Salvador, J. J. Dannenberg, S. Dapprich, A. D. Daniels, O. Farkas, J. B. Foresman, J. V. Ortiz, J. Cioslowski, D. J. Fox, *Gaussian16*, Gaussian, Inc., Wallingford, CT **2016**.
[40] P. Hohenberg, W. Kohn, *Phys. Rev.* **1964**, *136*, B864.
[41] W. Kohn, L. J. Sham, *Phys. Rev.* **1965**, *140*, A1133.
[42] J. Kohanoff, N. Gidopoulos, Density functional theory: basics, new trends and applications. in *Handbook of Molecular Physics and Quantum Chemistry*, Vol. 2, John Wiley & Sons Ltd., Chichester **2003**, p. 532.
[43] R. G. Parr, Density functional theory of atoms and molecules. in *Horizons of Quantum Chemistry*, Springer, Dordrecht **1980**, p. 5.
[44] J. P. Perdew, K. Burke, M. Ernzerhof, *Phys. Rev. Lett.* **1996**, *77*, 3865. https://doi.org/10.1103/PhysRevLett.77.3865.
[45] G. Lippert, J. Hutter, M. Parinello, *Mol. Phys.* **1997**, *92*, 477.
[46] J. Vandevondele, M. Krack, F. Mohamed, M. Parrinello, T. Chassaing, J. Hutter, *Comput. Phys. Commun.* **2005**, *167*, 103.
[47] S. Goedecker, M. Teter, J. Hutter, *Phys. Rev. B* **1996**, *54*, 1703.
[48] C. Hartwigsen, S. Gœdecker, J. Hutter, *Phys. Rev. B* **1998**, *58*, 3641.
[49] J. VandeVondele, J. Hutter, *J. Chem. Phys.* **2007**, *127*, 114105.
[50] S. Grimme, J. Antony, S. Ehrlich, H. Krieg, *J. Chem. Phys.* **2010**, *132*, 154104.
[51] M. Iannuzzi, A. Laio, M. Parrinello, *Phys. Rev. Lett.* **2003**, *90*, 238302.
[52] A. Laio, F. L. Gervasio, *Rep. Prog. Phys.* **2008**, *71*, 126601.
[53] A. Barducci, M. Bonomi, M. Parrinello, *Wiley Interdiscip. Rev.: Comput. Mol. Sci.* **2011**, *1*, 826.
[54] B. Ensing, A. Laio, M. Parrinello, M. L. Klein, *J. Phys. Chem. B* **2005**, *109*, 6676.
[55] V. Agarwal, P. J. Dauenhauer, G. W. Huber, S. M. Auerbach, *J. Am. Chem. Soc.* **2012**, *134*, 14958.
[56] R. Sun, O. Sode, J. F. Dama, G. A. Voth, *J. Chem. Theory Comput.* **2017**, *13*, 2332.
[57] M. McCullagh, M. G. Saunders, G. A. Voth, *J. Am. Chem. Soc.* **2014**, *136*, 13053.
[58] N. Vithani, S. Batra, B. Prakash, N. N. Nair, *ACS Catal.* **2017**, *7*, 902.
[59] A. Barducci, G. Bussi, M. Parrinello, *Phys. Rev. Lett.* **2008**, *100*, 020603.
[60] R. M. O'Ferrall, *J. Chem. Soc. B Phys. Orga.* **1970**, 274.
[61] W. P. Jencks, *Chem. Rev.* **1972**, *72*, 705.
[62] B. Ma, C. Meredith, H. F. Schaefer III., *J. Phys. Chem.* **1995**, *99*, 3815.
[63] C. H. Hu, T. Brinck, *J. Phys. Chem. A* **1999**, *103*, 5379.
[64] F. Ramirez, J. F. Marecek, J. Szamosi, *J. Org. Chem.* **1980**, *45*, 4748.
[65] J. Franck, E. Rabinowitsch, *Trans. Faraday Soc.* **1934**, *30*, 120.
[66] E. Rabinowitch, W. Wood, *Trans. Faraday Soc.* **1936**, *32*, 1381.
[67] N. Agmon, *Chem. Phys. Lett.* **1995**, *244*, 456.
[68] G. Zundel, H. Metzger, *Z. Phys. Chem.* **1968**, *58*, 225.
[69] M. Eigen, *Angew. Chem. Int. Ed.* **1964**, *3*, 1.
[70] D. Marx, M. E. Tuckerman, J. Hutter, M. Parrinello, *Nature* **1999**, *397*, 601.
[71] R. M. Noyes, *J. Chem. Phys.* **1954**, *22*, 1349.
[72] D. L. Miller, F. Westheimer, *J. Am. Chem. Soc.* **1966**, *88*, 1507.
[73] S. J. Admiraal, D. Herschlag, *Chem. Biol.* **1995**, *2*, 729.
[74] A. P. Carvalho, B. Leo, *J. Gen. Physiol.* **1967**, *50*(1327), 1327.
[75] C. W. Bock, A. Kaufman, J. P. Glusker, *Inorg. Chem.* **1994**, *33*, 419.
[76] F. C. Lightstone, E. Schwegler, R. Q. Hood, F. Gygi, G. Galli, *Chem. Phys. Lett.* **2001**, *343*, 549.
[77] I. Persson, *Pure Appl. Chem.* **2010**, *82*, 1901.
[78] A. K. Katz, J. P. Glusker, S. A. Beebe, C. W. Bock, *J. Am. Chem. Soc.* **1996**, *118*, 5752.
[79] S. L. Friess, *J. Am. Chem. Soc.* **1953**, *75*, 323.
[80] C. Kötting, K. Gerwert, *Chem. Phys.* **2004**, *307*, 227.
[81] T. Rudack, F. Xia, J. Schlitter, C. Kötting, K. Gerwert, *Biophys. J.* **2012**, *103*, 293.
[82] M. A. van Bochove, G. Roos, C. F. Guerra, T. A. Hamlin, F. M. Bickelhaupt, *Chem. Commun.* **2018**, *54*, 3448.

[83] A. S. Mildvan, C. M. Grisham, The role of divalent cations in the mechanism of enzyme catalyzed phosphoryl and nucleotidyl transfer reactions. in *Biochemistry*, Springer, Berlin, Heidelberg **1974**, p. 1.
[84] A. Kirby, W. Jencks, *J. Am. Chem. Soc.* **1965**, *87*, 3209.

SUPPORTING INFORMATION

Additional supporting information may be found online in the Supporting Information section at the end of this article.

How to cite this article: Saxena R, Avanigadda V B K Sai Phani Kumar, Singh R, Agarwal V. Ab initio dynamics of gas-phase and aqueous-phase hydrolysis of adenosine triphosphate. *Int J Quantum Chem*. 2021;121:e26615. https://doi.org/10.1002/qua.26615